2014-10

Effect of polyvinyl alcohol on the shape, photoluminescence and photocatalytic properties of PbMoO4 microcrystals

Materials Science in Semiconductor Processing, Amsterdam : Elsevier,v. 26, p. 425-430, Oct. 2014
http://www.producao.usp.br/handle/BDPI/50896

Materials Science in Semiconductor Processing 26 (2014) 425–430

Contents lists available at ScienceDirect

Materials Science in Semiconductor Processing

journal homepage: www.elsevier.com/locate/mssp

Effect of polyvinyl alcohol on the shape, photoluminescence and photocatalytic properties of $PbMoO_4$ microcrystals

V.D. Araújo [a,*], R.L. Tranquilin [b], F.V. Motta [a], C.A. Paskocimas [a], M.I.B. Bernardi [d], L.S. Cavalcante [e], J. Andres [c], E. Longo [b], M.R.D. Bomio [a]

[a] LSQM – Laboratório de Síntese Química de Materiais – DEMat, Universidade Federal do Rio Grande do Norte – UFRN, P.O. Box 1524, 59078-97 Natal, RN, Brazil
[b] LIEC, Universidade Federal de São Carlos – UFSCar, P.O. Box 676, 13565-905 São Carlos, SP, Brazil
[c] Departamento de Química Física y Analítica, Universitat Jaume I, 12071 Castello, Spain
[d] Instituto de Física de São Carlos, Universidade de São Paulo, USP, 13560-970 São Carlos, SP, Brazil
[e] Universidade Estadual do Piauí, Departamento de Química – CCN, Rua João Cabral, P.O. Box 2231, 64002-150 Teresina, PI, Brazil

ARTICLE INFO

Keywords:
$PbMoO_4$
Photocatalysis
Hydrothermal
PVA
Rhodamine B
Microcrystals

ABSTRACT

For this study, lead molybdate ($PbMoO_4$) microcrystals were prepared by the co-precipitation method and processed using a conventional hydrothermal method at 100 °C for 10 min with polyvinyl alcohol (PVA) as the capping agent. These microcrystals were structurally characterized by X-ray diffraction (XRD) and micro-Raman spectroscopy, and their morphology was investigated by field-emission gun scanning electron microscopy (FEG-SEM). The optical properties were analyzed by ultraviolet–visible (UV–vis) absorption spectroscopy and photoluminescence (PL) measurements. XRD patterns and MR spectrum indicate that the $PbMoO_4$ microcrystals have a scheelite-type tetragonal structure. FE-SEM images reveal that the PVA promotes the aggregation of several octahedrons and the formation of large porous stake-like $PbMoO_4$ microcrystals which are related to the oriented attachment growth process. Moreover, the effect of the capping agent hinders the growth of a large amount of micro-octahedrons which can be verified with by several nanocrystals on large crystals. Intense green PL emission was observed at room temperature for $PbMoO_4$ microcrystals which are related to structural defects at medium range and intermediary energy levels between the valence band (VB) and the conduction band (CB). Photocatalytic activity was observed for $PbMoO_4$ as a catalyst in the degradation of the rhodamine B (RhB) dye, achieving total degradation after 90 min under UV-light.

1. Introduction

Lead molybdate ($PbMoO_4$) crystals belong to the large family of alkaline earth metal molybdates with a general formula ($AMoO_4$) where A represents divalent cations (Ca^{2+}, Sr^{2+}, Ba^{2+} and Pb^{2+}) with a scheelite-type tetragonal structure and a space group of ($I4_1/a$) at room temperature [1]. These materials have attracted attention from the scientific community in the scientific literature due to their significant potential for different industrial applications such as birefringent filters [2], scintillation detectors [3], photoconductivity [4], fiber optics [5], luminescence [6–11], thermoluminescence [12,13] and photocatalysis [14,15].

In order to obtain $PbMoO_4$ structures, many synthetic techniques have been exploited such as classic solid state

* Corresponding author. Tel.: +55 84 3342 2260; fax: +55 84 3342 2406.
E-mail address: vicodantas@yahoo.com.br (V.D. Araújo).

http://dx.doi.org/10.1016/j.mssp.2014.05.027
1369-8001/

reaction [16], Czochralski crystal growth [17], galvanic cell method [18], citrate complex [19], and sonochemical route [20–22]; more facile preparations have been developed, including microemulsion method [23], microwave-assisted synthesis method [24,25], precipitation method [26,27], solvothermal route [7,28] and hydrothermal method [10,14,29,30], but these methods require the introduction of organics as templates, the use of surfactants, complexing agents and/or mineralizers which tend to complicate the synthetic procedure and may interfere with the photocatalytic performance of the as-synthesized materials [31,32]. A significant challenge still remains: to control the synthesized $PbMoO_4$ crystals with homogenous and well defined morphologies via facile routes. Among the chemical synthesis methods, the hydrothermal process has several advantages in terms of the control of synthesis parameters, especially the possibility of crystallization at mild temperatures and in liquid media, including the addition of templates or additives which produces samples with different morphologies and structures in a simple manner [31,33–36].

Similar to several technological applications of micro- and nanostructured materials, photocatalytic performance is related to factors such as morphology, size, crystalline phase, dopants and activity of specific crystalline plane [31,37–40]. Photocatalytic processes occur on the surface of catalysts, and thus, the size, shape and exposed crystal facets of crystals are essential in the activity and efficiency of photocatalysts; engineering the shapes of functional materials to desirable morphologies has long been actively pursued. The exposed facet of the $PbMoO_4$ crystal is an important factor which influences its photocatalytic performance for the degradation of pollutants such as organic dyes. The essence of exposed facets is the surface atomic configuration and coordination which affect the adsorption and reactivity of semiconductor materials [14]; in particular, studies on the photocatalytic activity of $PbMoO_4$ for the degradation of organic pollutants under UV light irradiation have been reported by different authors [28,30,41–46].

In our previous research, we studied the morphology and blue PL emission of $PbMoO_4$ [10]; in a more recent paper, the growth mechanism, infrared/Raman spectroscopies and PL properties of $PbMoO_4$ crystals obtained by the hydrothermal method have been reported [11]. In addition, a complimentary combination of experimental work and first principles calculations was carried out to obtain a deeper insight into the enhanced photocatalytic activity of $PbMoO_4$ crystals with predominant (111), (100), (011), and (110) facets [14].

Therefore, in this study, as a continuation of previous studies, we obtained $PbMoO_4$ (PMO) microcrystals by the co-precipitation (CP) method and processed by the hydrothermal method with PVA being the capping agent. These micro-octahedrons were analyzed by X-ray diffraction (XRD), micro-Raman spectroscopy, ultraviolet–visible (UV–vis) absorption spectroscopy, photoluminescence (PL) spectroscopy and field-emission gun scanning electron microscopy (FEG-SEM). The photocatalytic activity of the material was evaluated for degradation reactions of rhodamine B (RhB).

2. Experimental

2.1. Synthesis of $PbMoO_4$ microcrystals

All chemicals used were analytical grade reagents without further purification, $PbMoO_4$ (PMO) crystals were obtained by CP and hydrothermal methods with polyvinyl alcohol (PVA) (Vetec) as the capping agent. The typical synthesis procedure is described as follows: 0.005 mol of molybdic acid (H_2MoO_4) (Synth), 0.005 mol of lead nitrate [$Pb(NO_3)_2$] (Merck) and 0.1 g of PVA were dissolved in 75 mL of deionized water. Then 5 mL of ammonium hydroxide (NH_4OH) (30% in NH_3, Synth) was added to the solution until the pH value reached 10. These suspensions were stirred for 10 min in an ultrasound bath at room temperature.

This obtained suspension was transferred into a stainless steel autoclave (lined with quartz glass) which was sealed and processed at 100 °C for 10 min using a heating rate fixed at 2 °C/min. After hydrothermal processing, the autoclave was cooled down to room temperature. The resulting suspensions were washed several times with deionized water to neutralize the solution to pH (≈ 7); the white precipitates were dried with acetone and finally collected for characterization.

2.2. Characterization of $PbMoO_4$ microcrystals

After hydrothermal processing at 100 °C for 10 min, PMO crystals were structurally characterized by XRD using a Rigaku-DMax/2500PC (Japan) with Cu-Kα radiation (λ= 1.5406 Å) in the 2θ range from 10° to 75° with scanning rate of 0.02°/s and total exposure time of 15 min. Micro-Raman measurements were recorded using a T-64000 spectrometer (Jobin-Yvon, France) triple monochromator coupled to a CCD detector at 488 nm wavelength of an argon ion laser. Its maximum output power was kept at 10 mW with the use of lens (100 μm) to prevent sample overheating. Morphologies were investigated using FEG-SEM (Carl Zeiss, Supra 35-VP Model, Germany) operated at 6 kV. UV–vis spectra were taken using a Varian spectrophotometer, (Cary 5G Model, USA) in a diffuse reflection mode with MgO as the standard. PL measurements were carried out through a Monospec 27 monochromator (Thermal Jarrel Ash, USA) coupled to a R446 photomultiplier (Hamamatsu Photonics, Japan). A krypton ion laser (Coherent Innova 90K, USA) (λ=350 nm) was used as an excitation source, and its maximum output power was maintained at 500 mW; the maximum power maintained on the sample after passing through the optical chopper was 40 mW. All measurements were performed at room temperature.

2.3. Photocatalytic activity measurement

Photocatalytic properties of PMO crystals (as catalyst agents) for the degradation of rhodamine B (RhB) dye with a molecular formula of [$C_{28}H_{31}ClN_2O_3$] (99.5% purity, Mallinckrodt) in an aqueous solution were tested under UV-light illumination. About 50 mg of catalyst crystals were placed in a 250 mL beaker, and 50 mL of RhB solution (1×10^{-5} mol L^{-1}) was added at pH 4. These suspensions

were ultrasonicated for 10 min in an ultrasonic cleaner before illumination and were then stored in dark for 5 min to allow the saturated absorption of RhB onto the catalyst. The beakers were then placed in a photo-reactor at 20 μC and illuminated by six UV lamps (TUV Philips, 15 W with maximum intensity at 254 nm). The power light was measured (Coherent Power Max No. PM10 Model), and the optical energy density value was 20 mW cm^{-2}. At two-minute intervals, one 3 mL aliquot of these suspensions was removed and centrifuged at 9000 rpm for 5 min to remove crystals in suspension. Finally, variations of the maximum absorption band of supernatant solutions were monitored by UV–vis absorbance spectra measurements using a double-beam spectrophotometer with double monochromator and a JASCO photomultiplier tube detector (Model V-660, USA).

3. Results and discussion

Fig. 1 shows all PMO microcrystal XRD patterns which can be indexed to a scheelite-type tetragonal structure with a space group of ($I4_1/a$) and a point-group symmetry of (C_{4h}^6) which is in agreement with Inorganic Crystal Structure Database (ICSD) no. 26784. XRD peaks are intense and well defined which suggests a good degree of structural order at long range.

Fig. 2 shows Raman spectra of samples that complement the structural characterization. Group theoretical considerations suggest 13 Raman-active modes at the Γ point [47,48]:

$$\Gamma(\text{Raman}) = \upsilon_1(A_g)+\upsilon_2(A_g)+\upsilon_2(B_g)+\upsilon_3(B_g)+\upsilon_3(E_g) + \upsilon_4(B_g)+\upsilon_4(E_g)+\text{R}(A_g)+\text{R}(E_g)+2T(B_g)+2T(E_g) \quad (1)$$

Raman-active vibrational modes (A_g and B_g symmetry) are single modes while the E_g symmetry is doubly degenerated. Translational (T) modes and rotational (R) modes are considered to be external modes of tetrahedral [MoO_4] clusters and are the smallest in frequency. The modes

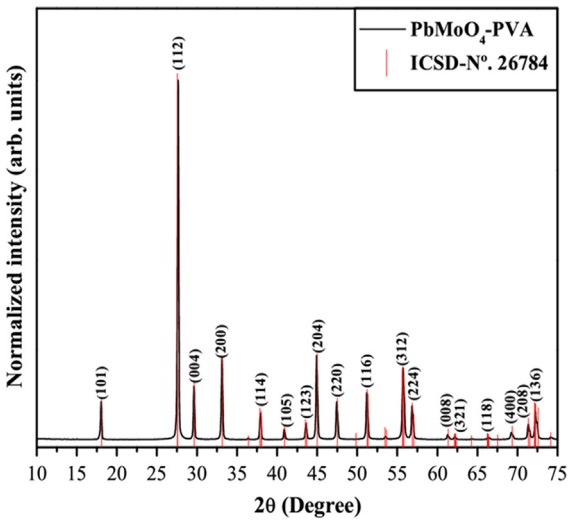

Fig. 1. XRD patterns of $PbMoO_4$ samples synthesized with PVA as the capping agent at 100 °C.

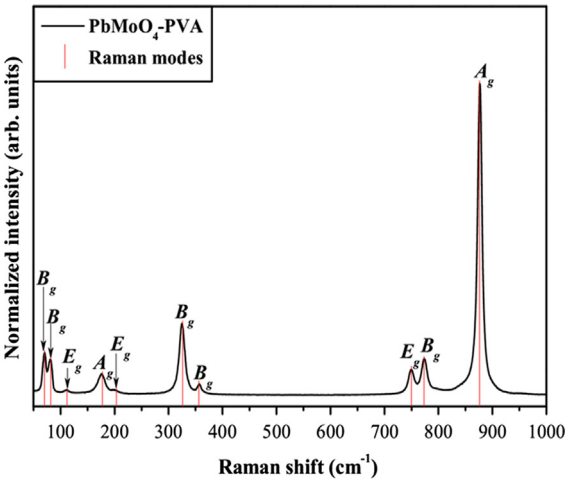

Fig. 2. Raman spectra of $PbMoO_4$ samples synthesized with PVA as the capping agent at 100 °C.

(υ_1 to υ_4) are considered to be the internal modes (stretching and bending) of tetrahedral [MoO_4] clusters and are higher in frequency, being the stretching modes the highest in frequency [48].

An analysis of the results indicates that all Raman-active modes of $PbMoO_4$ samples are characteristic of a tetragonal structure which is in agreement with results previously reported in the literature [49,50]. As seen in samples synthesized without the use of PVA [10,11,14], small shifts observed on Raman mode positions can be the result of different factors such as preparation methods, average crystal size, distortions involving the O–Mo–O and O–Pb–O moieties, interaction forces between the ions or the degree of structural order in the lattice [10]. Moreover, well defined active-Raman modes confirm that $PbMoO_4$ is structurally ordered at short-range.

The morphologic behavior of as-obtained PMO microcrystals was investigated by FEG-SEM images (see Fig. 3(a)–(d)) which confirm that PMO microcrystals have a large quantity of anisotropic microcrystals with octahedron-like shapes (see Fig. 3(a)); several quasi-spherical PMO nanocrystals are under large PMO microcrystals (see Fig. 3(b)). In addition, the initial growth process of these crystals produces large porous stake-like PMO microcrystals by using PVA as the capping agent through a self-organization of adjacent microcrystals in a similar crystallographic orientation "oriented attachment" process [51,52] along the [001] direction [10] which is followed by a subsequent coalescence process among these porous stake-like PMO microcrystals (see Fig. 3(c) and (d)). In fact, a similar previous mechanism established that PMO microcrystals with a scheelite-type structure that is composed of Pb^{2+} ions tend to be faceted and aligned by "docking" processes involving crystallographic fusion between faces with high surface energy which creates an extended morphology [10,53]. Also, PVA is essential for the formation of these porous stake-like PMO microcrystals. Researchers have found that PVA is a non-ionic polymer which is efficient only for binding metal cations to form a strong metal-binding ligand through a deprotonation process with high alkaline conditions [54–56]; due to its molecular chain, this process

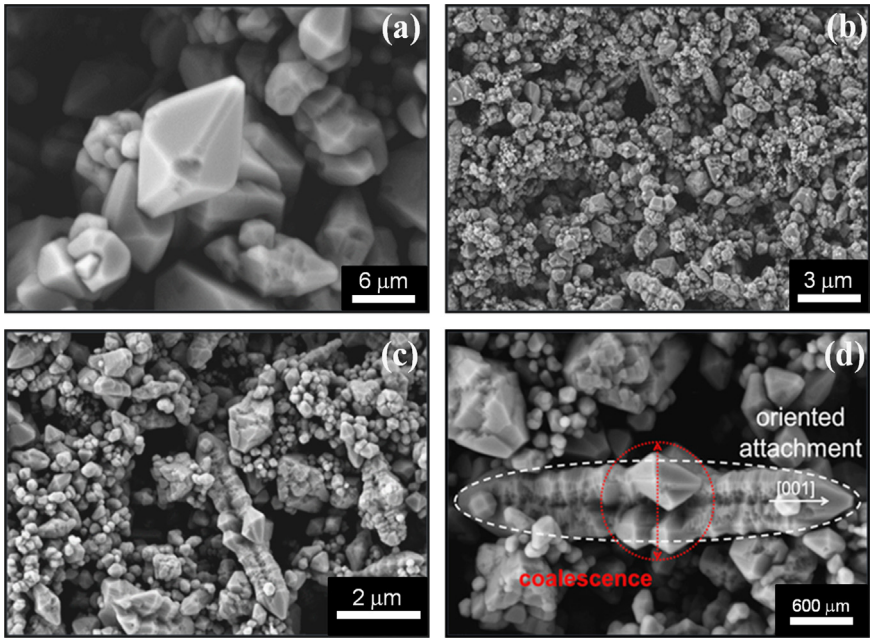

Fig. 3. (a–d) FEG-SEM images of PMO microcrystals synthesized with PVA as the capping agent.

can induce the formation of porous stake-like PMO microcrystals and quasi-spherical PMO nanocrystals [57–60]. Thus, we confirmed the effect of PVA as the capping agent, because we did not observed this morphological behavior in pure PMO microcrystals (Supporting information, Fig. SI-1(a,b)).

Fig. 4 shows the photoluminescence spectra of the PMO microcrystals obtained with an excitation wavelength of 325 nm. A simple Gaussian fit of the PL curve for PMO microcrystals is also illustrated (dashed curves) while the inset shows the optical band gap energy (E_{gap}) calculated by the method proposed by Wood and Tauc [61]. From the absorption edges, the band gap of as-obtained $PbMoO_4$ samples was estimated to be 3.15 eV which is in good agreement with band gap values obtained in data previously reported [10,14].

The Gaussian fit performed for PMO microcrystal PL emission reveals that this luminescence spectrum is formed by blue (495 nm – 33.04%), green (540 nm – 44.30%) and orange (600 nm – 22.66%) contributions with a maxima centered around 520 nm (green region). Several papers discuss the origin of PL emission in molybdates and tungstates crystalline structures. When excited with high-energy radiation (such as ultraviolet), these systems show a characteristic blue–green emission related to tetrahedral $[MoO_4]$ clusters for molybdates or tetrahedral $[WO_4]$ clusters for tungstates [62–64]. The origin of the green PL emission is controversial and is sometimes related to intrinsic transitions of the $[MoO_4]$ complex [65]. Based on our previous report [10], the PL emission obtained with maximum green intensity is due to locally distorted tetrahedral $[MoO_4]$ clusters and deltahedral $[PbO_8]$ clusters in the tetragonal lattice.

To demonstrate the photocatalytic activity of PMO microcrystals synthesized with PVA as the capping agent at 100 °C for 10 min, photodegradation of RhB dye was carried out in an aqueous dispersion (RhB dyes+PMO

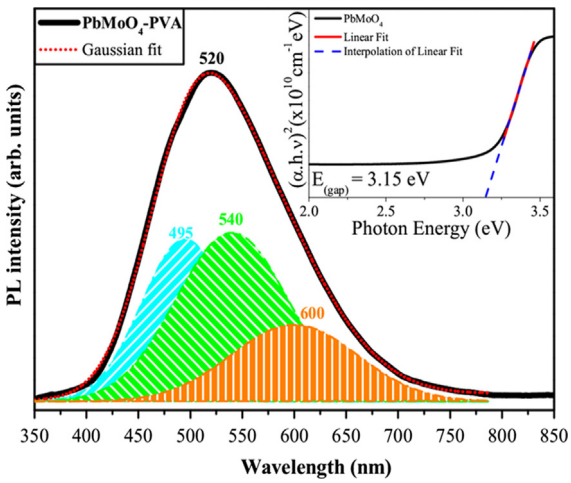

Fig. 4. PL spectrum of PMO microcrystals synthesized with PVA as the capping agent at 100 °C. The dashed lines represent a Gaussian profile fit for the $PbMoO_4$ sample. Inset shows the optical band gap estimated from UV–visible spectra.

catalyst) under UV light with the maximum intensity at 254 nm. The temporal evolution of adsorption and photocatalytic degradation of aqueous RhB dye solution is shown in Fig. 5.

As can be seen in Fig. 5, the RhB dye was totally photodegraded after 90 min under UV light illumination (see the inset of Fig. 5). A previous study [14] reported the photocatalytic activity of PMO microcrystals synthesized with different types of modifiers such as acetylacetone (ACAC) or polyvinylpyrrolidone (PVP) as well as PMO microcrystals without any modifier. That study verified that the RhB dye was totally photodegraded after 14 min for a sample synthesized with ACAC, 45 min for a sample

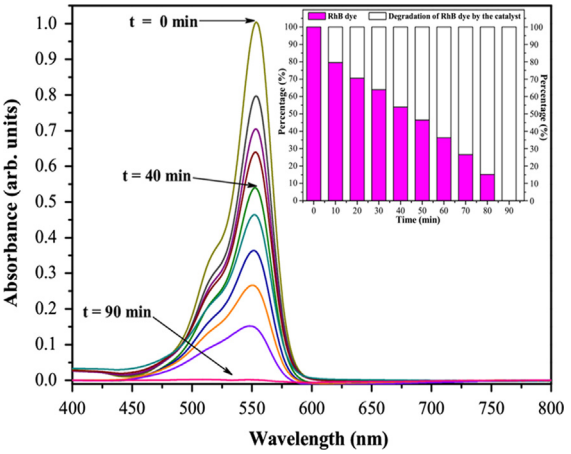

Fig. 5. UV–vis absorption spectra for $PbMoO_4$ sample synthesized with PVA as the capping agent during different exposure time of illumination for the photodegradation of RhB dyes. Inset shows photodegradation efficiencies of RhB dyes as a function of irradiation time.

with PVP and 55 min for PMO microcrystals synthesized without any modifier (Supporting information, Fig. SI-2). These results suggest that the photocatalytic enhancement of PMO microcrystals with ACAC as the capping agent (system without the (001) surface) could be related to surface/bulk defects that can influence the separation of photogenerated electron–hole pairs on PMO crystals under irradiation as well as exposed high-energy (111), (100), (011), and (110) facets.

In the work presented here, the photocatalytic formation is explained in terms of photo-generated electron–hole pair (excitons) processes and electronic transition between the valence band and the conduction band [14]. Initially, we assume that before the UV excitation reaches the system, the $PbMoO_4$ catalyst has the ability to generate electron–hole pairs. This behavior can be related to a reduction of band gap energy and an increase in the electronic intermediate levels between conduction and valence bands. Therefore, a considerable reduction in the optical band-gap is probably linked to exchange ordered complex clusters to disordered complex clusters. In this typical semiconductor, the $PbMoO_4$ crystal lattice can have different types of electronic structure characteristics such as intercluster (intermediary range) and intracluster (local range) interactions, which can be due to three different sources: orientation, induction, and dispersion interactions [66]. The orientation interaction is associated with correlation between rotational motion of permanent moments in different $[MoO_4]o$–$[MoO_4]d$ or $[PbO_8]o$–$[PbO_8]d$ complex clusters (medium range), where o=order and d=disorder. The induction interaction occurs via polarization processes of $[MoO_4]$ or $[PbO_8]$ clusters (short range). The dispersion interaction arises from correlation between electrons situated in the neighborhood of $[MoO_4]$ or $[PbO_8]$ clusters (long range). The cluster-to-cluster charge transfer (CCCT) in $PbMoO_4$ crystal containing more than one kind of cluster is characterized by excitations involving electronic transitions from one cluster to another. Therefore, these defects which are caused by $[MoO_4]o$, $[MoO_4]d$, $[PbO_8]o$ and $[PbO_8]d$ complex clusters can polarize in the lattice and lead to possible electronic transitions between disordered clusters and ordered clusters. In our model, the most important events occur before the arrival of the photon. Thus, different surfactants, temperatures and synthesis methods may affect the photocatalysis time due to formation of different short, medium and long distance defects. The clusters formed by $PbMoO_4$ interact with water and separate it into hydroxyl radicals and hydrogen ions. These radicals exhibit high oxidation power and produce mineralization of an organic compound in water.

It is still challenging to correlate surface defects with photocatalytic activity, because there are many other important effects such as crystalline phases, exposed crystal facets, etc. Therefore, the photocatalytic activity of PMO microcrystals is associated with the balance between all these factors; however it is rational to investigate the sole effect of defects on the photocatalytic activity of PMO microcrystals if other factors remain unchanged [14]. Thus, the lower photocatalytic activity of PMO microcrystals synthesized with PVA as the capping agent compared to pure PMO microcrystals or PMO microcrystals with ACAC as the capping agent and PMO microcrystals with PVP as the capping agent [14] could be related to structural defects in our samples which originate from the oriented attachment growth process and to less exposed active surfaces due to the formation of large porous stake-like PMO microcrystals (shown in Fig. 3(d)).

4. Conclusions

In summary, PMO microcrystals were obtained by the co-precipitation method and processed at 100 °C for 10 min in a conventional hydrothermal system with PVA as the capping agent. XRD patterns and micro-Raman spectrum indicate that PMO microcrystals have a scheelite-type tetragonal structure without deleterious phases. These results suggested that these structures are well ordered at long- and short-ranges. FEG-SEM images show that PMO microcrystals have a large quantity of anisotropic microcrystals with octahedron-like shapes or quasi-spherical PMO nanocrystals under the large PMO microcrystals which form large porous stake-like PMO microcrystals. The RhB dye was totally photodegraded after 90 min under UV light illumination. These results indicate that our PMO microcrystals have lower photocatalytic activity than that of pure PMO microcrystals synthesized without surfactant or as the capping agent. This behavior can be related to the minor exposed active surfaces due to the formation of large porous stakes-like PMO microcrystals via an oriented attachment process.

Acknowledgments

The authors thank the financial support from the following Brazilian research financing institutions: CNPq, FAPESP-CDMF Processo no. 2013/07296-2, CAPES AUX PE-PNPD-2280/2011. RECAM (Rede de Pesquisa em Catalisadores Ambientais) Processo no. 564913/2010-3; MCT/CNPq no. 74/2010 and Universal 14/2011 Processo no. 481288/2011-2. J.A. acknowledges Generalitat Valenciana Prometeo/2009/053 and Ministerio de Economía y Competitividad (Spain) (CTQ2012-36253-C03-02), and the Spanish–Brazilian Program (PHB2009-0065-PC) for their financial support.

Appendix A. Supporting information

Supplementary data associated with this article can be found in the online version at http://dx.doi.org/10.1016/j.mssp.2014.05.027.

References

[1] I. Trabelsi, M. Dammak, R. Maâlej, M. Kamoun, Physica B: Condens. Matter 406 (2011) 315–318.
[2] V.I. Skomorovsky, Proc. SPIE 2265 (1994) 413–421.
[3] M. Minowa, K. Itakura, S. Moriyama, W. Ootani, Nucl. Instrum. Methods Phys. Res. Sect. A 320 (1992) 500–503.
[4] H. Bernhardt, R. Schnell, Phys. Status Solidi A 64 (1981) 207–214.
[5] E.W. Taylor, A.D. Sanchez, S.A. DeWalt, R.J. Padden, S.P. Chapman, T. W. Monarski, et al., Proc. SPIE 1794 (1993) 217–224.
[6] Y.A. Hizhnyi, S.G. Nedilko, J. Lumin. 102–103 (2003) 688–693.
[7] H. Alves, A. Hofstaetter, F. Leiter, B.K. Meyer, N.G. Romanov, R. Novotny, et al., Radiat. Meas. 33 (2001) 641–644.
[8] J.A. Groenink, G. Blasse, J. Solid State Chem. 32 (1980) 9–20.
[9] D.A. Spassky, S.N. Ivanov, V.N. Kolobanov, V.V. Mikhailin, V. N. Zemskov, B.I. Zadneprovski, et al., Radiat. Meas. 38 (2004) 607–610.
[10] J.C. Sczancoski, M.D.R. Bomio, L.S. Cavalcante, M.R. Joya, P.S. Pizani, J. A. Varela, et al., J. Phys. Chem. C 113 (2009) 5812–5822.
[11] M.R.D. Bomio, L.S. Cavalcante, M.A.P. Almeida, R.L. Tranquilin, N. C. Batista, P.S. Pizani, et al., Polyhedron 50 (2013) 532–545.
[12] W. Bollmann, Kristall Tech. 15 (1980) 367–375.
[13] A. Hofstaetter, R. Oeder, A. Scharmann, D. Schwabe, B. Vitt, Phys. Status Solidi B 89 (1978) 375–380.
[14] M.R.D. Bomio, R.L. Tranquilin, F.V. Motta, C.A. Paskocimas, R. M. Nascimento, L. Gracia, et al., J. Phys. Chem. C 117 (2013) 21382–21395.
[15] A. Kudo, M. Steinberg, A. Bard, A. Campion, M. Fox, T. Mallouk, et al., Catal. Lett. 5 (1990) 61–66.
[16] H.C. Zeng, J. Mater. Res. 11 (1996) 703–715.
[17] H.C. Zeng, J. Cryst. Growth 160 (1996) 119–128.
[18] P.K. Pandey, N.S. Bhave, R.B. Kharat, Indian J. Pure Appl. Phys. 44 (2006) 52–58.
[19] J.H. Ryu, S.-M. Koo, J.-W. Yoon, C.S. Lim, K.B. Shim, Mater. Lett. 60 (2006) 1702–1705.
[20] A. Phuruangrat, T. Thongtem, S. Thongtem, Curr. Appl. Phys. 10 (2010) 342–345.
[21] G. Kianpour, M. Salavati-Niasari, H. Emadi, Ultrason. Sonochem. 20 (2013) 418–424.
[22] L. Yang, Y. Wang, Y. Wang, X. Wang, G. Han, J. Ceram. Soc. Jpn. 120 (2012) 609–612.
[23] D. Chen, G. Shen, K. Tang, Z. Liang, H. Zheng, J. Phys. Chem. B 108 (2004) 11280–11284.
[24] A. Phuruangrat, T. Thongtem, S. Thongtem, J. Cryst. Growth 311 (2009) 4076–4081.
[25] P. Kwolek, T. Tokarski, T. Lokcik, K. Szacilowski, Arch. Metall. Mater. 58 (2013) 217–222.
[26] T. Thongtem, S. Kungwankunakorn, B. Kuntalue, A. Phuruangrat, S. Thongtem, J. Alloys Compd. 506 (2010) 475–481.
[27] G. Kianpour, M. Salavati-Niasari, H. Emadi, Superlattices Microstruct. 58 (2013) 120–129.
[28] G.-J. Xing, R. Liu, C. Zhao, Y.-L. Li, Y. Wang, G.-M. Wu, Ceram. Int. 37 (2011) 2951–2956.
[29] Y. Cheng, Y. Wang, D. Chen, F. Bao, J. Phys. Chem. B 109 (2004) 794–798.
[30] M. Shen, Q. Zhang, H. Chen, T. Peng, CrystEngComm 13 (2011) 2785–2791.
[31] T.M. Milao, V.R. de Mendonça, V.D. Araujo, W. Avansi, C. Ribeiro, E. Longo, et al., Sci. Adv. Mater. 4 (2012) 54–60.
[32] T.R. Giraldi, G.V.F. Santos, V.R. Mendonça, C. Ribeiro, I.T. Weber, J. Nanosci. Nanotechnol. 11 (2011) 3635–3640.
[33] M. Yoshimura, K. Byrappa, J. Mater. Sci. 43 (2008) 2085–2103.
[34] F. Zhou, X.M. Zhao, C.G. Yuan, L. Li, Cryst. Growth Des. 8 (2008) 723–727.
[35] W. Avansi, C. Ribeiro, E.R. Leite, V.R. Mastelaro, Cryst. Growth Des. 9 (2009) 3626–3631.
[36] W. Avansi, C. Ribeiro, E.R. Leite, V.R. Mastelaro, Mater. Chem. Phys. 127 (2011) 56–61.
[37] M.R. Hoffmann, S.T. Martin, W. Choi, D.W. Bahnemann, Chem. Rev. 95 (1995) 69–96.
[38] U.I. Gaya, A.H. Abdullah, J. Photochem. Photobiol. C: Photochem. Rev. 9 (2008) 1–12.
[39] C. Guillard, J. Disdier, J.-M. Herrmann, C. Lehaut, T. Chopin, S. Malato, et al., Catal. Today 54 (1999) 217–228.
[40] M. Itoh, T. Kajitani, Phys. Rev. B 87 (2013) 085201–085209.
[41] D.B. Hernández-Uresti, A. Martínez-de la Cruz, L. Torres-Martínez, Res. Chem. Intermed. 38 (2012) 817–828.
[42] A. Martínez-de la Cruz, D.B. Hernández-Uresti, L. Torres-Martínez, S. W. Lee, React. Kinet. Mech. Catal. 107 (2012) 467–475.
[43] D.B. Hernandez-Uresti, J.A. Aguilar-Garib, A. Martinez-de la Cruz, J. Microw. Power Electromagn. Energy 46 (2012) 163–173.
[44] Y. Shimodaira, H. Kato, H. Kobayashi, A. Kudo, Bull. Chem. Soc. Jpn. 80 (2007) 885–893.
[45] K. Dai, Y. Yao, H. Liu, I. Mohamed, H. Chen, Q. Huang, J. Mol. Catal. A: Chemical 374 (2013) 111–117.
[46] D.B. Hernandez-Uresti, A. Martinez-de la Cruz, J.A. Aguilar-Garib, Catal. Today 212 (2013) 70–74.
[47] S.P.S. Porto, J.F. Scott, Phys. Rev. 157 (1967) 716–719.
[48] R. Vilaplana, O. Gomis, F.J. Manjon, P. Rodriguez-Hernandez, A. Munoz, D. Errandonea, et al., J. Appl. Phys. 112 (2012) 103510.
[49] Y. Cuiling, Y. Qingjiang, G. Chunxiao, L. Bao, H. Aimin, H. Chunyuan, et al., J. Phys.: Condens. Matter 19 (2007) 425215.
[50] A. Jayaraman, B. Batlogg, L.G. VanUitert, Phys. Rev. B 31 (1985) 5423–5427.
[51] R.L. Penn, J.F. Banfield, Science 281 (1998) 969–971.
[52] X. Peng, L. Manna, W. Yang, J. Wickham, E. Scher, A. Kadavanich, et al., Nature 404 (2000) 59–61.
[53] H. Colfen, S. Mann, Angew. Chem. Int. Ed. 42 (2003) 2350–2365.
[54] Y.-M. Hu, H.-S. Gu, D. Zhou, Z. Wang, HL-W Chan, Y. Wang, J. Am. Ceram. Soc. 93 (2010) 609–613.
[55] U. Paik, V.A. Hackley, J. Lee, S. Lee, J. Mater. Res. 18 (2003) 1266–1274 .
[56] K. Hegetschweiler, Chem. Soc. Rev. 28 (1999) 239–249.
[57] H.Y. He, W.P. Lao, J.F. Huang, J. Ceram. Process. Res. 11 (2010) 485–489.
[58] Z. Guo, F. Du, G. Li, Z. Cui, Cryst. Growth Des. 8 (2008) 2674–2677.
[59] X. Yao, X. Xin, Y. Zhang, J. Wang, Z. Liu, X. Xu, J. Alloys Compd. 521 (2012) 95–100.
[60] N. Murakami, S. Kawakami, T. Tsubota, T. Ohno, J. Mol. Catal. A: Chemical 358 (2012) 106–111.
[61] D.L. Wood, J. Tauc, Phys. Rev. B 5 (1972) 3144–3151.
[62] V.V. Laguta, J. Rosa, M.I. Zaritskii, M. Nikl, Y. Usuki, J. Phys.: Condens. Matter 10 (1998) 7293–7302.
[63] M. Martini, F. Meinardi, G. Spinolo, A. Vedda, M. Nikl, Y. Usuki, Phys. Rev. B 60 (1999) 4653–4658.
[64] A.A. Blistanov, B.I. Zadneprovskii, M.A. Ivanov, V.V. Kochurikhin, V. S. Petrakov, I.O. Yakimova, Crystallogr. Rep. 50 (2005) 284–290.
[65] Z.D. Lou, M. Cocivera, Mater. Res. Bull. 37 (2002) 1573–1582.
[66] D.C. Cronemeyer, Phys. Rev. 113 (1959) 1222–1226.